Carbohydrate Polymers 93 (2013) 144–153

Contents lists available at SciVerse ScienceDirect

Carbohydrate Polymers

journal homepage: www.elsevier.com/locate/carbpol

Property evaluations of dry-cast reconstituted bacterial cellulose/tamarind xyloglucan biocomposites

Clayton F. de Souza[a,b], Neoli Lucyszyn[a,1], Marco A. Woehl[a], Izabel C. Riegel-Vidotti[a], Redouane Borsali[b], Maria Rita Sierakowski[a,*]

[a] BioPol, Departamento de Química, Universidade Federal do Paraná (UFPR), P.O. 19081, Curitiba 81531-980, PR, Brazil
[b] Centre de Recherche sur les Macromolécules Végétales (CERMAV) Domaine Universitaire de Grenoble-St Martin d'Hères, 601 rue de la chimie, CERMAV-CNRS, BP 53, 38041 Grenoble cedex 9, France

ARTICLE INFO

Article history:
Received 30 October 2011
Received in revised form 30 March 2012
Accepted 24 April 2012
Available online 4 May 2012

Keywords:
Bacterial cellulose
Xyloglucan
Polysaccharide interactions
Biocomposite
Surface properties
Hydrophilicity

ABSTRACT

We describe the mechanical defibrillation of bacterial cellulose (BC) followed by the dry-cast generation of reconstituted BC films (RBC). Xyloglucan (XGT), extracted from tamarind seeds, was incorporated into the defibrillated cellulose at various compositions, and new films were created using the same process. Microscopy and contact angle analyses of films revealed an increase in the microfibre adhesion, a reduced polydispersity in the diameters of the microfibrils and increased hydrophobic behaviour as a function of %XGT. X-ray diffraction analysis revealed changes to the crystallographic planes of the RBC and the biocomposite films with preferential orientation along the (1 1 0) plane. Compared with BC, RBC/XGT biocomposite with 10% XGT exhibited improvement in its thermal properties and in Young's modulus. These results indicated a reorganisation of the microfibres with mechanical treatment, which when combined with hydrocolloids, can create cellulose-based materials that could be applied as scaffolding for tissue engineering and drug release.

1. Introduction

The versatility of biopolymers allows for new applications in the food, pharmaceutical and biotechnology industries. The structures and functionalities of polysaccharides, proteins and lipids allow their utilisation in biomimetic and nanotechnology systems, including biosensors, transistors or mechanical modifiers. Cellulose is one of the most studied biopolymers, and several sources of this biopolymer have been evaluated. The backbone chains of cellulose, consisting of long linear chains of 1,4-β-D-glucopyranose, are organised by hydrogen bonds that form a hard network structure. This linearity yields multiple elementary fibrils that aggregate into larger bundles, which can contain crystalline and amorphous regions. The degrees of crystallinity and the crystal dimensions are dependent on the origin of the cellulose or on the modification (chemical or physical) to which it was submitted (Guo & Catchmark, 2012; Sugiyama, Vuong, & Chanzy, 1991; Tischer, Sierakowski, Westfahl, & Tischer, 2010; Wong, Kasapis, & Tan, 2009; Woodcock & Sarko, 1980). Specifically, cellulose from bacterial sources exhibits higher crystallinity and has distinct advantages over cellulose from other sources. These advantages include high purity (pretreatment is not required for the extraction of lignin or hemicelluloses) and high surface area when compared with plant cellulose (Guo & Catchmark, 2012). Therefore, the great interest in bacterial cellulose (BC) is justified by its many potential applications. These applications include medical devices (Nge, Nogi, Yano, & Sugiyama, 2010) and wound dressings to prevent infection caused by bacterial or fungal agents that can occur as skin heals (Czaja, Young, Kawecki, & Brown, 2007; Jonas & Farah, 1998).

Many of the functional properties of cellulose depend on its capacity to interact with diverse molecules or macromolecules of varying polarity. The adsorption and adhesion phenomena depend on the organisation of glucan chains located at the surface of the cellulose microfibrils (Mazeau, 2011). The association of hydrophilic structures, including hydrocolloids such as xyloglucan, with cellulose can modify the mechanical and chemical properties of the cellulose (Zhou, Rutland, Teeri, & Brumer, 2007). The structural description of the cellulose microfibril surfaces or that of cellulose associated with other molecules can be performed using several techniques. Recent studies include atomic force microscopy (AFM), scanning electron microscopy (SEM), contact angle (CA) measurements and small- and wide-angle X-ray diffraction (SAXS and WAXS) (Castro et al., 2011; Elazzouzi-Hafraoui et al., 2008;

* Corresponding author. Tel.: +55 41 33613260; fax: +55 41 33613186.
E-mail address: mariarita.sierakowski@ufpr.br (M.R. Sierakowski).
[1] Present address: Curso de Licenciatura em Química, Escola de Educação e Humanidades, Pontifícia Universidade Católica do Paraná (PUCPR) Curitiba 80215-901, PR, Brazil.

0144-8617/$ – see front matter © 2012 Elsevier Ltd. All rights reserved.
http://dx.doi.org/10.1016/j.carbpol.2012.04.062

Huang, Chen, Lin, Hsu, & Chen, 2010; Klechkovskaya et al., 2003; Woehl et al., 2010). The results have provided information regarding the morphology on various scales, the hydrophilicity-related properties, the microfibril dimensions and the relative crystallinity of these cellulose samples.

Recent advances in computer modelling and surface force analysis have improved our understanding of the cellulose chains and the cellulose–xyloglucan interactions at the molecular level (Mazeau, 2011; Zhang, Brumers, Agren, & Tu, 2011). *In vitro*, these complex structures are important to many applications particularly in the biotech industries. Some studies have demonstrated that cellulose-based films, after processing, show selective permeability, allowing the passage of water vapour while preventing the passage of microorganisms (Chang & Zhang, 2011; Klemm et al., 2009).

A commercial xyloglucan product isolated from tamarind seeds (*Tamarindus indica*) has important applications, especially in pharmaceutical formulations to obtain gels (Salazar-Montoya, Ramos-Ramírez, & Delgado-Reyes, 2002; Yamanaka et al., 2000), and as a drug vehicle for controlled-release systems (Burgalassi, Chetoni, Panichi, Boldrini, & Saettone, 2000; Coviello, Matricardi, Marianecci, & Alhaique, 2007; Jó, Petri, Beltramini, Lucyszyn, & Sierakowski, 2010; Kawasaki et al., 1999; Miyazaki, Kawasaki, Endo, & Attwood, 2001). This biopolymer is formed by a 1,4-β-D-glucopyranosyl backbone partially substituted with 1,6-α-D-xylopyranosyl side chains, some of which are further substituted with 1,2-α-D-galactopyranosyl residues (Freitas et al., 2005; Hayashi, 1989; Jó, Petri, Valenga, Lucyszyn, & Sierakowski, 2009; Muller et al., 2011; Stupp et al., 2008; York, Harvey, Guillen, Albersheim, & Darvill, 1993).

In addition, because xyloglucan (XG) has storage or structural functions in plants, its association with cellulose has been widely studied in relation to biosynthesis and the growth process of higher plant organisms (Zhou et al., 2007). These studies have enabled new discoveries and applications based on the cellulose–xyloglucan interaction. For example, the development of XG as a molecular anchor to tether chemical functionality to cellulose opened new possibilities for industrial plant fibre modification in which it is used as a dispersing agent or to build nanostructured surfaces (Muller et al., 2011; Zhou et al., 2007). In all cases, the cellulose–xyloglucan interaction is slightly dependent on its structural details as observed by Lopez et al. (2010). The authors observed that the adsorption is dependent on M_w and on the side chains.

The development of biocomposites from cellulose and other additives has been widely explored. However, the methodologies typically used include a pretreatment of the cellulose, which involves a rigorous process of solubilisation and reconstruction of the cellulose membrane. Thus, the purpose of this research is to use bacterial cellulose (BC) in the development of films by first mechanically defibrillating and reconstructing the cellulose *via* a dry-cast process to produce RBC. In addition, the inclusion of tamarind XG as a substitute for defibrillated BC pulp was explored at varying percentages to produce biocomposite films with distinct properties. The structural, morphological, thermal and mechanical stabilities were evaluated using several techniques. The results obtained can promote new methods for the production of cellulose-based materials for use in, among other applications, tissue engineering support and drug release.

2. Materials and methods

2.1. Polysaccharide sources

Prior to the dry-cast process, the xyloglucan was obtained from *T. indica* seeds by aqueous extraction from tamarind kernel powder (TKP, Balasanka Mills, India) with an approximately 55–65% recovery of the polysaccharide (Menon et al., 2010). The chemical composition of the TKP used in the present work has been previously reported (Jó et al., 2009, 2010).

The TKP was dispersed in distilled water at 30 °C and stirred overnight, then sonicated for 30 min using a solid 25-mm probe (VCX 750, Sonics & Materials, Inc., Newton, CT, USA). The insoluble fraction was separated by centrifugation at 6311 × *g*, and the soluble fraction was precipitated with the addition of commercial ethanol (98%, Dipalcool Distribuidora de Álcool Ltda, Almirante Tamandaré, PR, Brazil), washed with acetone and dried in an oven at 50 °C. Then, the purified xyloglucan (XGT) was characterised by gel permeation chromatography (GPC), in a Viscotek 270 Dual Detector GPC, with PWxl columns (2500, 4000 and 6000 g/mol), at 30 °C using 0.1 mol/L $NaNO_3$ with 0.02% (w/v) NaN_3 as an eluent and a *dn*/*dc* increment of 0.144.The never-dried bacterial cellulose (BC) cultured from *Acetobacter xylinum* was donated by Membracel Produtos Tecnológicos Ltda®, located at Almirante Tamandaré, PR, Brazil. Because the BC was received in the presence of hypochlorite and acetic acid, neutralisation was performed, and the membranes were dialysed against distilled water. The conductivity and pH were monitored until constant values (~4.8 μS/cm and ~6.8) were obtained. Finally, the material was washed several times with ultrapure water. For comparative purposes, dried commercial BC from the same company was used as a control in all experiments.

2.2. Achievement of dry-cast cellulose biocomposites

The never-dried BC (99 wt% of water) (Klemm et al., 2009) was submitted to mechanical treatment to yield a pulp using a blade mixer over 30 min. To this, 2 L ultrapure water was added for each 20 g of wet BC.

Various volumes of an aqueous XGT solution were incorporated into the pulp to yield final compositions of 10, 20 or 30 wt%.

The dispersions, deposited on polypropylene petri dishes, were oven dried for 48 h at 37 °C to yield RBC or biocomposite films.

2.3. Biocomposite characterisations

2.3.1. Scanning electron microscopy (SEM) and atomic force microscopy (AFM) analysis

The SEM images were obtained using a JEOL JSM-6360LV microscope (JEOL Ltd., Tokyo, Japan) at 10 kV and at a magnification of 10,000×. All samples were covered by a thin layer of gold (<10 nm) to improve the conductivity of the surface.

The AFM analyses were performed on an Agilent microscope (Agilent Technologies, Santa Clara, CA, USA) using Pico Image software (Agilent Technologies, Santa Clara, CA, USA). The tapping mode images were obtained with Vistaprobes® (Nanoscience Instruments, Inc., Phoenix, AZ, USA) silicon tips (nominal spring of 48 N/m and resonance frequency of ~180 kHz), and the scanning was over 2.0 μm × 2.0 μm and 5.0 μm × 5.0 μm. The data treatment and presentation were accomplished with the help of Gwyddion Software (Czech Metrology Institute).

2.3.2. Contact angle (CA) analysis

The CA analysis was obtained in a DataPhysics GmbH tensiometer (Filderstadt, Germany), model OCA 15plus. A study of the hydrophilicity on the surface of the biocomposites was performed using the sessile drop method with ultrapure water as the solvent. The measurements were conducted at 25 °C using a 500-μL Hamilton syringe (Bonaduz, Switzerland) and a needle with an internal diameter of 1.37 mm, an external diameter of 1.65 mm and a length of 38.1 mm.

The surface free energy was obtained using Young's equation with the contact angle results. The calculation was performed with

SCA 20 DataPhysics software (San Jose, CA, USA) and the results were obtained by averaging at least three measurements.

2.3.3. X-ray diffraction (XRD)

The X-ray diffraction patterns of the BC, RBC and the biocomposite films were analysed with a Shimadzu XRD-7000 diffractometer (Kyoto, Japan) with Ni-filtered Cu Kα radiation (λ = 0.15418 nm, 40 kV, 30 mA). The diffractograms were obtained in a 2θ-range from 10° to 30° at a scanning rate of 1.5°/min. The *d-spacing* was obtained using Bragg's law and the crystal size (CS) using Scherrer's equation as follows:

$$n\lambda = 2d \cdot \sin\theta$$

$$\mathrm{CS} = \frac{0.9 \cdot \lambda}{\mathrm{FWHM} \cdot \cos\theta}$$

in which n is an integer, λ is the wavelength of the incident wave, d is the spacing between the plane lattices, θ is the angle between the incident ray and the scattering planes and the FWHM (in radians) is the width of the peak at half the maximum height (Castro et al., 2011; Elazzouzi-Hafraoui et al., 2008).

The crystallinity index (CrI, %) was calculated using the following method described by Hermans, Hermans, Vermaas, and Weidinger (1948):

$$\mathrm{CrI}\,(\%) = \frac{A_{\mathrm{cryst}}}{A_{\mathrm{total}}} \times 100$$

The A_{cryst} is the sum of the crystalline area and A_{total} is the total area under the diffractograms (Poletto, Zattera, Forte, & Santana, 2012). All calculations were performed using Fityk software (Wojdyr, 2010), and the peaks were deconvoluted using the Gaussian peak function.

The contribution of the (1 1 0) plane to the diffractograms was calculated using the following equation:

$$(1\,1\,0)\mathrm{contribution} = \frac{A_{(1\,1\,0)}}{A_{\mathrm{cryst}}} \times 100\%$$

in which $A_{(1\,1\,0)}$ is the area of the deconvoluted (1 1 0) peak.

2.3.4. Thermogravimetric analysis (TG)

The experiments were carried out using a Setaram TGA92 (Setaram, France) with heating rate of 5.0 °C/min under a N_2 atmosphere (gas flow rate of 40 cm^3/min). Approximately 30 mg of each sample was placed into a quartz cell, and its thermal degradation was measured from 20 to 500 °C. To avoid interference from the equipment, a background analysis was performed using an empty quartz cell under the same conditions.

2.3.5. Mechanical properties

Tensile testing was performed in an Instron 5565 tensile testing system (Norwood, MA, USA) following the procedures outlined in the ASTM method D 882-95a. The tests were carried out in a humidity-controlled room with 50% relative humidity. Five-to-ten replicates of 10 mm in width and 30 mm in gage length (grip separation) were tested for each sample at a cross-head speed of 3 mm/min.

3. Results and discussion

3.1. Physicochemical parameters of XGT and the preparation of dry-cast biocomposites

The physicochemical characteristics of XGT as determined by a multi-detector GPC are provided in detail in Table S1 of the supplementary material. The number- and weight-average molar mass were determined to be 416.29×10^3 and 214.79×10^3 g/mol, respectively, which differ from the results of Freitas, Gorin, Neves, and Sierakowski (2003), Freitas et al. (2005) and Jó et al. (2009) who related higher values of 1.00×10^6 g/mol and 653.00×10^3 g/mol, respectively. These higher M_w results can be attributed to both the formation of supramolecular aggregates and the method of purification (Freitas et al., 2005; Picout, Ross-Murphy, Errington, & Harding, 2003). The physicochemical characteristics (see Table S1) are in good agreement with the results obtained by Picout et al. (2003), Freitas et al. (2005) and Muller et al. (2011), indicating good results for the GPC parameters, which demonstrate good solubilisation and low aggregation with the given purification conditions.

The reconstituted bacterial cellulose (RBC) and RBC/XGT biocomposites were used to form films *via* a dry-cast process. A scheme for the membrane production is proposed in Fig. 1. This process attempted the development of a material with similar characteristics of commercial BC and with new properties after XGT inclusion. This process attempted the development of a material with properties similar to commercial BC. Thus far, several projects have demonstrated synergism between xyloglucan and cellulose from a variety of sources, morphologically and chemically changing the cellulose matrix (Lopez et al., 2010; Zhou et al., 2007).

3.2. Scanning electron microscopy (SEM) and contact angle (CA) measurements

To determine the morphological aspects and surface effects of RBC and RBC/XGT films, SEM and CA analyses were performed. Visually, according to the images shown in Fig. 1, the BC and RBC/XGT exhibited the same appearance with a good dispersion and homogeneity. In contrast, the SEM images (Fig. 2) exhibited less homogeneous surfaces, with regions of high association between the cellulose microfibrils and a loss of porous regions (voids), indicating the adsorption of XGT, which provided a more compact association of the RBC microfibrils. However, all biocomposites exhibited the same "mesh-like" structure as others obtained through different drying processes. For example, reconstituted cellulose created using a freeze-drying process was observed by Sokolnicki, Fisher, Harrah, and Kaplan (2006), reconstituted cellulose created in the presence of chitin was reported by Liang, Zhang, and Xu (2007), and starch/reconstituted BC composites were described by Woehl et al. (2010). The properties of the films or composites obtained are dependent upon the conditions of the drying process. Therefore, a variety of features and morphologies can be achieved for different applications. Some authors obtained biofilters and scaffolds from cellulose-based materials using a freeze-drying process (Barroso, Temtem, Hussain, Aguiar-Ricardo, & Roque, 2010; Nge et al., 2010; Sokolnicki et al., 2006). Others inserted xyloglucan *in situ* into the production of the bacterial cellulose and observed different associations and ribbon sizes according to the xyloglucan concentration, which yielded a cellulose surface network with a variety of characteristics (Zhou et al., 2007).

The CA images and results obtained for the RBC and RBC/XGT films are shown in Fig. 2 and Table 2, respectively. As previously discussed, the SEM results indicated variations in the aggregation and porosity of the biocomposite surfaces as a function of XGT inclusion. In addition, the CA analysis revealed changes to the hydrophilicity of the surfaces. Based on the CA results, the surface free energy was obtained for the biocomposites, and the relationship between the surface free energy and the degree of XGT substitution was found, with 10% > 20% > 30%.

The native celluloses are formed by I_α and I_β allomorphs. In bacterial cellulose, the I_α allomorph occurs preferentially (Attala & Vanderhart, 1984). This allomorph is more hydrophilic than I_β due to its structure in which the hydroxyl groups are more susceptible to hydrogen interactions (Mazeau, 2011; Tischer et al., 2010). So, the surface of cellulose is a favourable environment for the

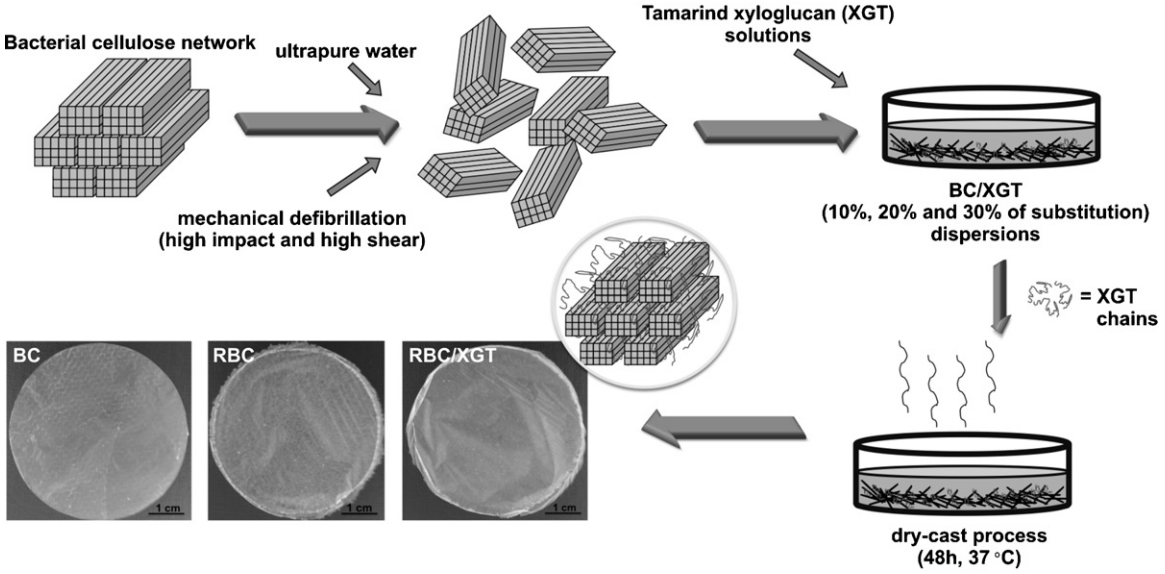

Fig. 1. Scheme for the production of biofilms of reconstituted bacterial cellulose (RBC) and RBC/tamarind xyloglucan (XGT) biocomposites by a dry-cast process.

intercalation of XGT, which also explains the loss of polarity on the surface. Fig. 2(c) and (d) shows regions with no evident fibrils, apart from sub-micrometre-sized round structures that may represent regions of XGT accumulation, which could also contribute to the changes in the hydrophilicity of the films.

3.3. Atomic force microscopy (AFM)

Through the topographic analysis of 5.0 μm × 5.0 μm images obtained by tapping-mode AFM (Fig. 3), the roughness values for all of the studied films could be calculated, and the results are

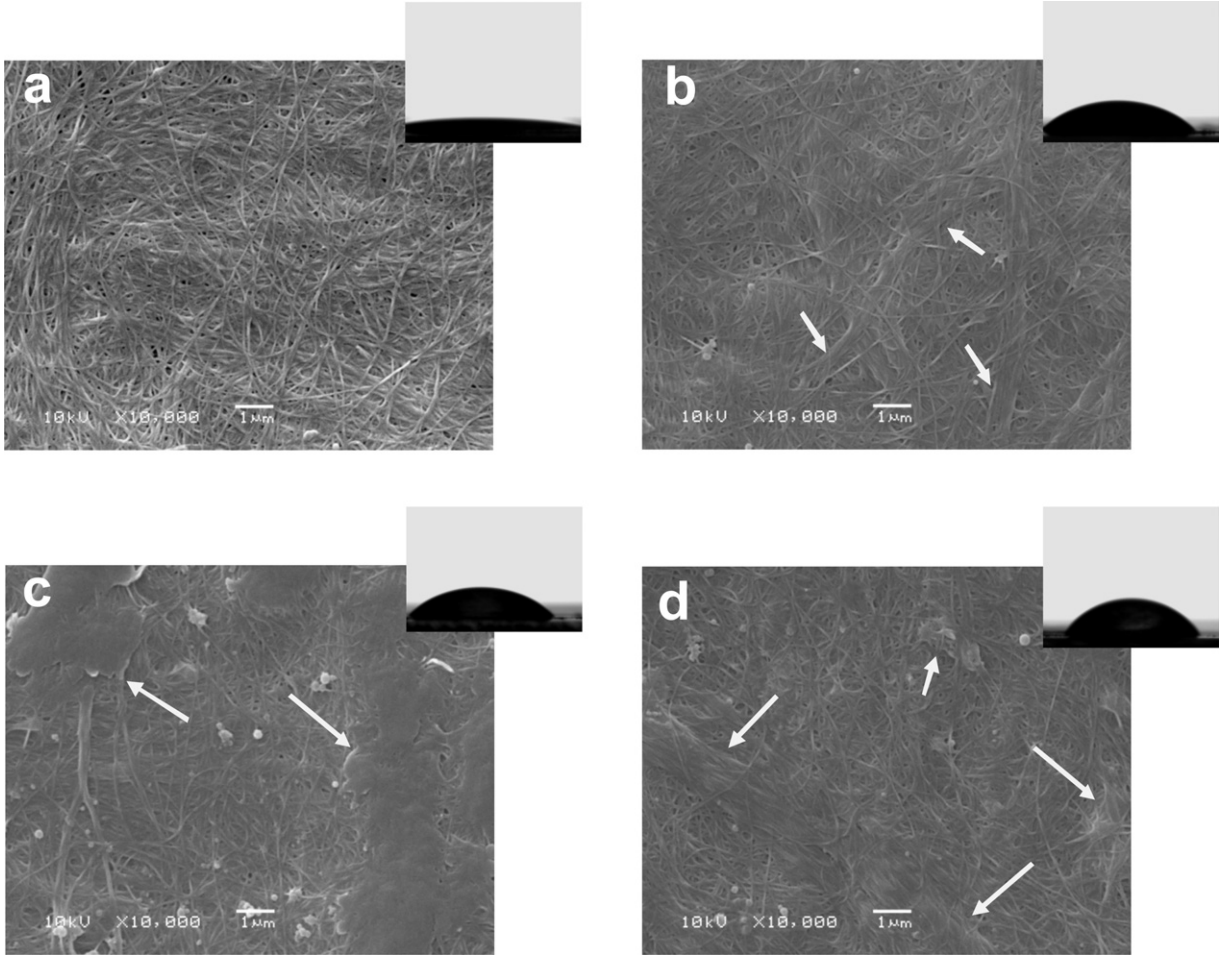

Fig. 2. SEM and CA images of biofilms of reconstituted bacterial cellulose – RBC (a) and RBC/tamarind xyloglucan (XGT) biocomposites with varying degrees of XGT substitution: 10% (b), 20% (c) and 30% (d). The arrows indicate aggregation zones.

Table 1
Crystallinity index (CrI)[a], crystallite size (CS)[a] and surface properties of biofilms of bacterial cellulose (BC), reconstituted bacterial cellulose (RBC), and RBC/tamarind xyloglucan (XGT) biocomposites with varying degrees of XGT substitution (%).

Samples	CrI (%)	CS_{100} (nm)	CS_{010} (nm)	CS_{110} (nm)	Roughness (nm)[b]	Contact angle (±0.1) (°)[c]	Surface free energy (±0.1) (mN/m)[d]
BC	83.27	2.82	3.81	5.63	6.77 (±0.83)	25.8	66.4
RBC	89.67	3.58	4.27	6.02	6.87 (±0.92)	11.9	71.2
RBC/XGT 10%	76.18	4.52	5.42	6.02	10.23 (±1.69)	45.8	56.1
RBC/XGT 20%	82.76	4.36	5.25	6.03	10.10 (±1.40)	49.4	54.1
RBC/XGT 30%	79.90	4.33	5.21	6.05	10.97 (±1.86)	58.7	48.6

[a] Using deconvoluted Gaussian curves on X-ray diffractograms.
[b] Root mean square values (rms) using 5.0 μm × 5.0 μm tapping-mode AFM images.
[c] By OCA 15plus tensiometer measurements using sessil drop method.
[d] By SCA 20 DataPhysics software using Young's equation method.

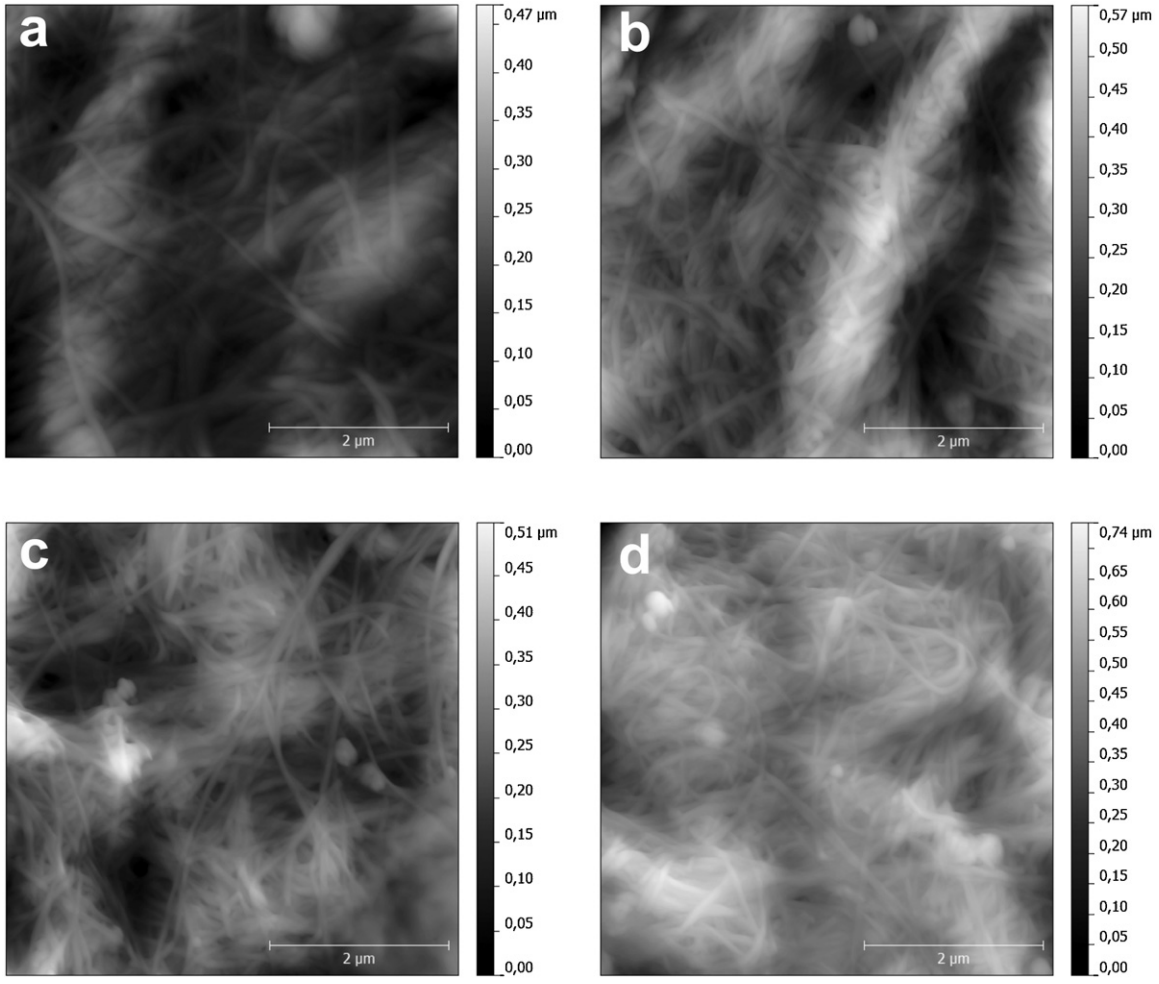

Fig. 3. AFM tapping-mode images (5.0 μm × 5.0 μm) of biofilms of reconstituted bacterial cellulose – RBC (a) and RBC/tamarind xyloglucan (XGT) biocomposites with varying degrees of substitution: 10% (b), 20% (c) and 30% (d).

presented in Table 1. In the presence of XGT the biocomposites are rougher than the controls (BC or RBC). Moreover, the association of the RBC microfibrils changes as a function of the hydrocolloid inclusion. The dispersion of the XGT was evident in a variety of cellulose associations.

A cross-sectional analysis of the topographic AFM-images at 2.0 μm × 2.0 μm (Fig. S1 in the supplementary material) indicates that no modification occurred in the microfibril width, which has a lateral size distribution between 50 and 100 nm, following the casting process. The dimensions of the blends are in agreement with the cellulose values obtained through a different process (Elazzouzi-Hafraoui et al., 2008; Klechkovskaya et al., 2003; Tischer et al., 2010). Furthermore, the RBC allowed more ribbon associations, and the inclusion of XGT caused a reduction in the polydispersity of the microfibril diameters.

The more homogeneous organisation of the microfibrils was observed by AFM, which could explain the change in the hydrophilicity of the biocomposites. The round-shaped features increasing in number from Fig. 3(b)–(d) may result from clusters of XGT that are not associated with the RBC fibrils. This result is

Table 2
Thermogravimetric (TG) results for biofilms of bacterial cellulose (BC), reconstituted bacterial cellulose (RBC), and RBC/tamarind xyloglucan (XGT) biocomposites with varying degrees of XGT substitution (%).

Sample	TG results			
	Moisture (%)	T_i [a] (°C)	DTG_{peak} [b] (°C)	Residual mass[c] (%)
BC	4.81	274.62	345.55	21.46
RBC	3.68	315.58	343.20	19.21
RBC/XGT 10%	4.34	307.30	346.22	22.05
RBC/XGT 20%	4.87	294.89	346.68	23.35
RBC/XGT 30%	5.31	294.89	343.57	23.07

[a] Onset temperature of the main thermal decomposition (organic fraction).
[b] Maximum derived peak on main thermal decomposition.
[c] Final mass at 500 °C.

consistent with the XGT accumulation as deduced from the SEM images.

3.4. X-ray diffraction analyses (XRD)

XRD is commonly used to study the crystallinity of cellulose. The source, the extraction and the treatment of the cellulose have each been shown to alter its crystallographic arrangements (Castro et al., 2011; Mishima, Hisamatsu, York, Teranishi, & Yamada, 1998; Nishiyama, 2009; Pérez & Samain, 2010). Tischer et al. (2010) studied the reorganisation of bacterial cellulose films following ultrasonic treatment, and their results indicated an increase in the crystallinity (and a reduction in the surface roughness).

XRD analysis was performed to observe some effects of crystallinity on RBC and biocomposite films, and the results are shown in Fig. 4. In each diffractogram, three defined peaks are observed at 14.61°, 16.90° and 22.73°, which corresponding to the (1 0 0), (0 1 0) and (1 1 0) planes, respectively, according to the Sugiyama indices (Sugiyama et al., 1991).

Using Bragg's equation, all exhibited the same *d-spacing*, *i.e.*, 0.61 nm (d_{100}), 0.53 nm (d_{010}) and 0.39 nm (d_{110}). Similar values were obtained by Klechkovskaya et al. (2003) and Castro et al. (2011) with bacterial cellulose produced by *A. xylinum* and *Gluconobacter swingsii* sp., respectively.

The relative intensity of the (1 1 0) peak (Fig. 4(f)) is smaller in BC than in RBC. This is a result of the fibres' orientation. The casting process allows the cellulose ribbons to lay with their larger surface parallel to the surface of the film, hence increasing the amount of X-ray radiation diffracted by the (1 1 0) face.

The XRD results also show that the inclusion of XGT led to changes in the crystalline arrangement of the RBC. First, in all of the biocomposites the peaks exhibit higher resolution than those of the controls, BC and RBC. Furthermore, in the biocomposites, the relative peak intensity of the (1 1 0) plane is even higher than in RBC, indicating that the XGT increases the orientation of the ribbons (Fig. 4(f)).

The peaks of the diffractograms were deconvoluted using a Gaussian function, and some structural information was obtained. For the RBC and RBC/XGT films, XRD patterns have shown a broad, low-intensity peak at approximately 20° that refers to the amorphous contribution of the biocomposites (Mishima et al., 1998).

The CrI (%) results (Table 1) do not significantly change the high crystallinity of the BC and biocomposites. In contrast, the CrI (%) of RBC was increased in comparison with the BC. This, in addition to the slightly larger crystallite sizes (CS) of the RBC and biocomposites in the (1 0 0) and (0 1 0) directions, may indicate a reorganisation of the microfibrils due to the mechanical disruption. A similar effect was observed by Tischer et al. (2010); following the ultrasonic treatment of BC, the direction and ribbon dimensions changed.

3.5. Thermogravimetric analysis (TG)

The thermal stability was studied with a cycle of degradation to 500 °C, and the results are shown in Fig. 5 and Table 2. The mass loss percentage was obtained from the TG plots, and the temperatures within which degradation occurs were estimated from the curves. We observed two well-defined events in all samples (Fig. 5(a)). The first (approximately 80–100 °C) was considered the loss of adsorbed water (moisture %), and in all cases, the moisture was approximately 3.5–4.9%. In addition, a linear increase was observed in the moisture as a function of the hydrocolloid concentration, indicating increased water retention in the biocomposites.

The second event (approximately 300–370 °C) refers to the degradation of the organic fraction with a high weight loss (greater than 70%). The dry-cast process generated materials with higher thermal stability than BC. However, the derived curves (Fig. 5(b)) indicate that the temperature of degradation (the DTG peak) exhibits no significant differences.

The DTG curves (Fig. 5(b)) shown for RBC indicate that the small event at 288.06 °C observed with BC (indicated by the arrow) was lost along with others that appeared with the biocomposites. The results for BC indicate that some ribbons are not completely associated on the cellulose matrix, and the decomposition process can be initiated at lower temperatures. In biocomposites, the small event at 294.89–307.93 °C (also indicated by an arrow) can be attributed to the decomposition of the XGT fraction (Poletto et al., 2012). Furthermore, no evidence of these events was found for RBC, indicating more favourable associations with the cellulose chains following the dry-cast process, which results in higher thermal stability. For all samples the residual mass was high (approximately 22–23%). The TG results are in agreement with those for cellulose from a variety of sources studied (Gao, Shen, & Lu, 2011; Jeon, Oh, Kee, & Kin, 2010; Poletto et al., 2012; Wong et al., 2009). These results indicate that the structural rearrangements observed in other analyses improve the stability of the cellulose matrix in RBC, and the optimum association is created through the dry-cast process.

3.6. Mechanical properties

Fig. 6(a) provides the typical stress/strain curves of BC, RBC and the biocomposites. The curve of the biocomposite with 10% XGT closely resembles the commercial sample in the low-strain region, and the Young's modulus (Fig. 6(b)) is higher than that for either BC or RBC. These results may be related to the formation of nanofibre bundles as shown in the AFM images (Fig. 3(a)). Thus, this behaviour suggests that the XGT provides adhesion between the fibres, thus improving their modulus in comparison with the RBC.

The RBC, in turn, has a lower tensile strength than the commercial BC (Fig. 6(c)). Although the imaging techniques applied did not allow an estimation of the fibre length, one may assume a shortening of the fibres due to mechanical defibrillation, thus reducing the fibre entanglement responsible for the elastic response in long-fibre composites (Dalmas, Cavaillé, Gauthier, Chazeau, & Dendievel, 2007; Samir, Alloin, & Dufresne, 2005). The addition of a small amount (10%) of XGT into the biocomposite partially compensates for the loss in tensile strength in the RBC, probably by providing a stress-transfer mechanism at the fibre/polymer interface (Dalmas, Chazeau, Gauthier, Cavaille, & Dendievel, 2006; Tjong, 2006).

For greater amounts of XGT, the strength enhancement is lost (Fig. 6(c)). The uneven fibre distribution in the composites with 20 and 30% XGT, which is evidenced by regions of XGT accumulation (SEM analysis, Fig. 2(c) and (d)), may be responsible for the loss of strength enhancement because in these regions the fibre–fibre interaction is reduced. In nanofibre composites, this interaction prevails over the fibre–matrix interactions (Dalmas et al., 2007).

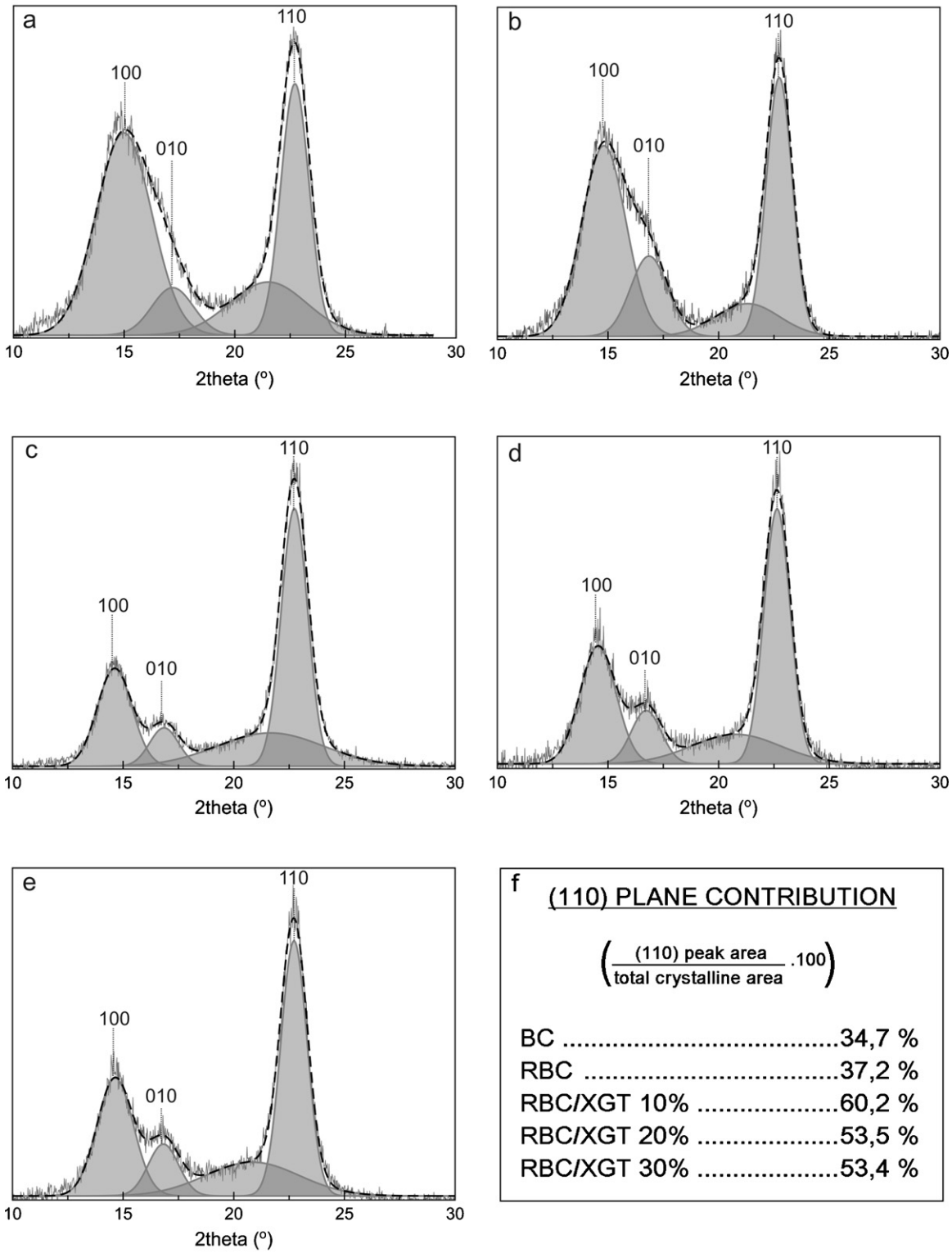

Fig. 4. X-ray diffractograms for biofilms of bacterial cellulose – BC (a), reconstituted bacterial cellulose – RBC (b), RBC/tamarind xyloglucan (XGT) biocomposites with varying degrees of XGT substitution: 10% (c), 20% (d) and 30% (e), and a (1 1 0) plane contribution calculated from these diffractograms (f).

The biocomposites exhibit a lower strain at break compared with the BC and RBC films, even those containing 10% XGT (Fig. 6(d)). This behaviour was already observed in other nanofibre–polymer composites (Varela-Rizo, Weisenberger, Bortz, & Martin-Gullon, 2010): the fibre network minimises crack initiation at low stress, but it is not efficient in preventing crack propagation. Therefore, the biocomposites in low-stress and low-strain situations exhibit mechanical behaviour comparable to BC and to a system developed as a scaffold for tissue engineering (Rambo et al., 2008). The biocomposites also exhibited better mechanical behaviour than a hydrocolloid membrane developed as skin substitute (Park et al., 2004).

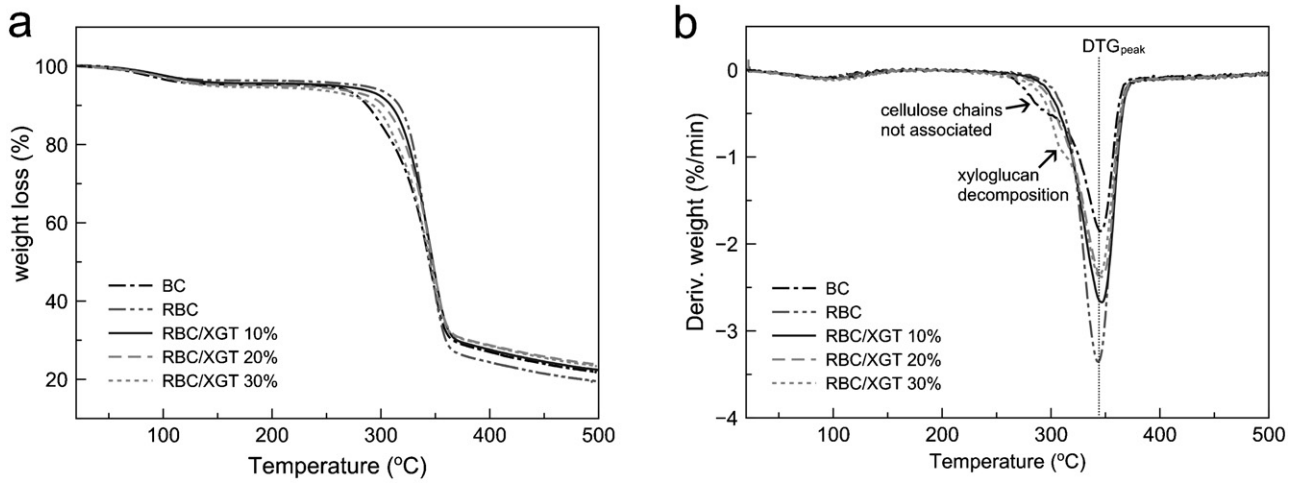

Fig. 5. TGA (a) and DTG (b) curves for biofilms of bacterial cellulose (BC), reconstituted bacterial cellulose (RBC) and RBC/XGT biocomposites with varying degrees of XGT substitution (%).

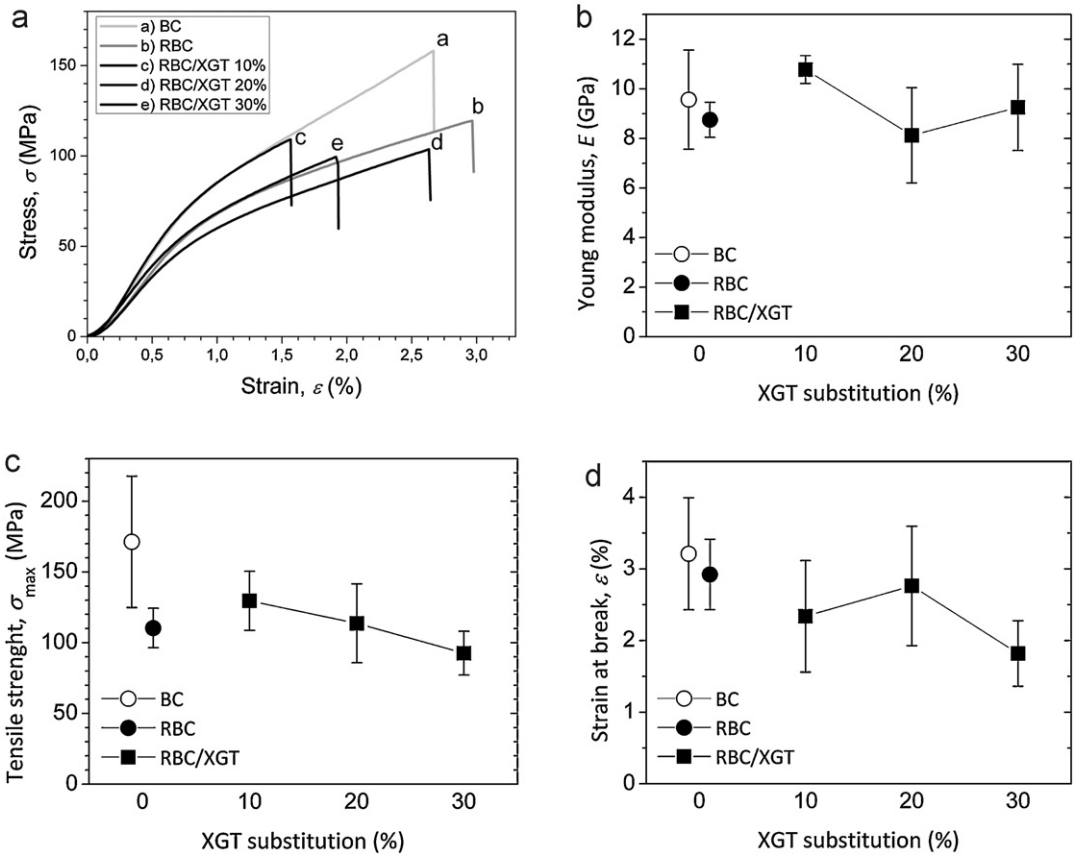

Fig. 6. Typical stress/strain curves (a), Young's modulus (b), tensile strength (c) and strain at break (d) for the biofilms of bacterial cellulose (BC), reconstituted bacterial cellulose (RBC) and RBC/XGT biocomposites with varying degrees of XGT substitution (%).

4. Conclusions

The mechanical disruption of BC and the development of an RBC biofilm using a dry-cast process produced better fibre association and orientation of the fibrils, which promoted higher thermal stability. With XGT inclusion, an increase in hydrocolloids promotes better fibre adhesion as observed by SEM and AFM. As a mechanical modifier, the presence of XGT (10%) increases the Young's modulus in a low strain as compared with BC and RBC, and probably promotes a stress-transfer mechanism in the fibre/polymer interface, which results in a performance similar to the BC film. The intrinsic properties of XGT on the biocomposite structure make it a programmable platform with increased roughness and a neutral background with respect to control or non-specific adhesion. These features could be utilised for biotechnological applications such as scaffolds for tissue engineering and drug release.

Acknowledgements

The authors acknowledge the Brazilian funding agencies, including CNPq (Conselho Nacional de Pesquisa) and Rede

Nanobiotec/CAPES-Brazil for financial support, and DFIS/UFPR and CERMAV for analysis support. The authors are grateful to Membracel Produtos Tecnológicos Ltda (Brazil) for providing the bacterial cellulose samples.

Appendix A. Supplementary data

Supplementary data associated with this article can be found, in the online version, at http://dx.doi.org/10.1016/j.carbpol.2012.04.062.

References

Attala, R. H., & Vanderhart, D. L. (1984). Native cellulose: A composite of two distinct crystalline forms. *Science*, *223*(4633), 283–285.

Barroso, T., Temtem, M., Hussain, A., Aguiar-Ricardo, A., & Roque, A. C. A. (2010). Preparation and characterization of a cellulose affinity membrane for human immunoglobulin G (IgG) purification. *Journal of Membrane Science*, *348*(1–2), 224–230.

Burgalassi, S., Chetoni, P., Panichi, L., Boldrini, E., & Saettone, M. F. (2000). Xyloglucan as a novel vehicle for timolol: Pharmacokinetics and pressure lowering activity in rabbits. *Journal Ocular Pharmacology and Therapeutics*, *16*(6), 497–509.

Castro, C., Zuluaga, R., Puteaux, J.-L., Caro, G., Mondragon, I., & Gañán, P. (2011). Structural characterization of bacterial cellulose produced by *Gluconobacter swingsii* sp. from Colombian agroindustrial wastes. *Carbohydrate Polymers*, *84*(1), 96–102.

Chang, C., & Zhang, L. (2011). Cellulose-based hydrogels: Present status and application prospects. *Carbohydrate Polymers*, *84*(1), 40–53.

Coviello, T., Matricardi, P., Marianecci, C., & Alhaique, F. (2007). Polysaccharide hydrogels for modified release formulations. *Journal of Controlled Release*, *119*(1), 5–24.

Czaja, W. K., Young, D. J., Kawecki, M., & Brown, R. M., Jr. (2007). The future prospects of microbial cellulose in biomedical applications. *Biomacromolecules*, *8*(1), 1–12.

Dalmas, F., Cavaillé, J.-Y., Gauthier, C., Chazeau, L., & Dendievel, R. (2007). Viscoelastic behavior and electrical properties of flexible nanofiber filled polymer nanocomposites. Influence of processing conditions. *Composites Science and Technology*, *67*(5), 829–839.

Dalmas, F., Chazeau, L., Gauthier, C., Cavaille, J. Y., & Dendievel, R. (2006). Large deformation mechanical behavior of flexible nanofiber filled polymer nanocomposites. *Polymer*, *47*(8), 2802–2812.

Elazzouzi-Hafraoui, S., Nishiyama, Y., Puteaux, J.-L., Heux, L., Dubreuil, F., & Rochas, C. (2008). The shape and size distribution of crystalline nanoparticles prepared by acid hydrolysis of native cellulose. *Biomacromolecules*, *9*(1), 57–65.

Freitas, R. A., Gorin, P. A. J., Neves, J., & Sierakowski, M.-R. (2003). A rheological description of mixtures of a galactoxyloglucan with high amylose and waxy corn starches. *Carbohydrate Polymers*, *51*(1), 25–32.

Freitas, R. A., Martin, S., Santos, G. L., Valenga, F., Buckeridge, M. S., Reicher, F., et al. (2005). Physico-chemical properties of seed xyloglucans from different sources. *Carbohydrate Polymers*, *60*(4), 507–514.

Gao, Q., Shen, X., & Lu, X. (2011). Regenerated bacterial cellulose fibers prepared by the NMMO·H_2O process. *Carbohydrate Polymers*, *83*(3), 1253–1256.

Guo, J., & Catchmark, J. M. (2012). Surface area and porosity of acid hydrolyzed cellulose nanowhiskers and cellulose produced by *Gluconacetobacter xylinus*. *Carbohydrate Polymers*, *87*(2), 1026–1037.

Hayashi, T. (1989). Xyloglucan in the primary cell wall. *Annual Review of Plant Physiology and Plant Molecular Biology*, *40*, 139–166.

Hermans, P. H., Hermans, J. J., Vermaas, D., & Weidinger, A. J. (1948). Deformation mechanism of cellulose gels. IV. General relationship between orientation of the crystalline and that of the amorphous portion. *Journal of Polymer Science*, *3*(1), 1–9.

Huang, H.-C., Chen, L.-C., Lin, S.-B., Hsu, C.-P., & Chen, H.-H. (2010). In situ modification of bacterial cellulose network structure by adding interfering substances during fermentation. *Bioresource Technology*, *101*(15), 6084–6091.

Jeon, J.-H., Oh, I.-K., Kee, C.-D., & Kin, S.-J. (2010). Bacterial cellulose actuator with electrically driven bending deformation in hydrated condition. *Sensors and Actuators B: Chemical*, *146*, 307–313.

Jó, T. A., Petri, D. F. S., Beltramini, L. M., Lucyszyn, N., & Sierakowski, M.-R. (2010). Xyloglucan nano-aggregates: Physico-chemical characterisation in buffer solution and potential application as a carrier for camptothecin, an anti-cancer drug. *Carbohydrate Polymers*, *82*(2), 355–362.

Jó, T. A., Petri, D. F. S., Valenga, F., Lucyszyn, N., & Sierakowski, M.-R. (2009). Thin films of xyloglucans for BSA adsorption. *Materials Science and Engineering C*, *29*(2), 631–637.

Jonas, R., & Farah, L. F. (1998). Production and application of microbial cellulose. *Polymer Degradation and Stability*, *59*(1–3), 101–106.

Kawasaki, N., Ohkura, R., Miyazaki, S., Uno, Y., Sugimoto, S., & Attwood, D. (1999). Thermally reversible xyloglucan gels as vehicles for oral drug delivery. *International Journal of Pharmaceutics*, *181*(2), 227–234.

Klechkovskaya, V. V., Baklagina Yu, G., Stepina, N. D., Khripunov, A. K., Buffat, P. A., Suvorova, E. I., et al. (2003). Structure of cellulose *Acetobacter xylinum*. *Crystallography Reports*, *48*(5), 755–762.

Klemm, D., Schumann, D., Kramer, F., Heßler, N., Koth, D., & Sultanova, B. (2009). Nanocellulose materials—Different cellulose, different functionality. *Macromolecular Symposia*, *280*(1), 60–71.

Liang, S., Zhang, L., & Xu, J. (2007). Morphology and permeability of cellulose/chitin blend membranes. *Journal of Membrane Science*, *287*(1), 19–28.

Lopez, M., Bizot, H., Chambat, G., Marais, M.-F., Zykwinska, A., Ralet, M.-C., et al. (2010). Enthalpic studies of xyloglucan–cellulose interactions. *Biomacromolecules*, *11*(6), 1417–1428.

Mazeau, K. (2011). On the external morphology of native cellulose microfibrils. *Carbohydrate Polymers*, *84*(1), 524–532.

Menon, V., Prakash, G., & Rao, M. (2010). Enzymatic hydrolysis and ethanol production using xyloglucanase and *Debaromyces hansenii* from tamarind kernel powder: Galactoxyloglucan predominant hemicellulose. *Journal of Biotechnology*, *148*(4), 233–239.

Mishima, T., Hisamatsu, M., York, W. S., Teranishi, K., & Yamada, T. (1998). Adhesion of β-D-glucans to cellulose. *Carbohydrate Research*, *308*(3–4), 389–395.

Miyazaki, N., Kawasaki, N., Endo, K., & Attwood, D. (2001). Oral sustained delivery of theophylline from thermally reversible xyloglucan gels in rabbits. *Journal of Pharmacy and Pharmacology*, *53*(9), 1185–1191.

Muller, F., Manet, S., Jean, B., Chambat, G., Boué, F., Heux, L., et al. (2011). SANS measurements of semifexible xyloglucan polysaccharide chains in water reveal their self-avoiding statistics. *Biomacromolecules*, *12*(9), 3330–3336.

Nge, T. T., Nogi, M., Yano, H., & Sugiyama, J. (2010). Microstructure and mechanical properties of bacterial cellulose/chitosan porous scaffold. *Cellulose*, *17*(2), 349–363.

Nishiyama, Y. (2009). Structure and properties of the cellulose microfibril. *Journal of Wood Science*, *55*(4), 241–249.

Park, S. N., Kim, J. K., & Suh, H. (2004). Evaluation of antibiotic-loaded collagen–hyaluronic acid matrix as a skin substitute. *Biomaterials*, *25*(17), 3689–3698.

Pérez, S., & Samain, D. (2010). Structure and engineering of celluloses. *Advances in Carbohydrate chemistry and Biochemistry*, *64*, 25–116.

Picout, D. R., Ross-Murphy, S. B., Errington, N., & Harding, S. E. (2003). Pressure cell assisted solubilization of xyloglucans: Tamarind seed polysaccharide and detarium gum. *Biomacromolecules*, *4*(3), 799–807.

Poletto, M., Zattera, A. J., Forte, M. M. C., & Santana, R. M. C. (2012). Thermal decomposition of wood: Influence of wood components and cellulose crystallite size. *Bioresource Technology*, *109*, 148–153.

Rambo, C. R., Recouvreux, D. O. S., Carminatti, C. A., Pitlovanciv, A. K., Antonio, R. V., & Porto, L. M. (2008). Template assisted synthesis of porous nanofibrous cellulose membranes for tissue engineering. *Materials Science & Engineering C: Biomimetic and Supramolecular Systems*, *28*(4), 549–554.

Salazar-Montoya, J. A., Ramos-Ramírez, E. G., & Delgado-Reyes, V. A. (2002). Changes of the dynamic properties of tamarind (*Tamarindus indica*) gel with different saccharose and polysaccharide concentrations. *Carbohydrate Polymers*, *49*(4), 387–391.

Samir, M., Alloin, F., & Dufresne, A. (2005). Review of recent research into cellulosic whiskers, their properties and their application in nanocomposite field. *Biomacromolecules*, *6*(2), 612–626.

Sokolnicki, A. M., Fisher, R. J., Harrah, T. P., & Kaplan, D. L. (2006). Permeability of bacterial cellulose membranes. *Journal of Membrane Science*, *272*(1–2), 15–27.

Stupp, T., Freitas, R. A., Sierakowski, M.-R., Deschamps, F. C., Wisniewski, A., Jr., & Biavatti, M. W. (2008). Characterization and potential uses of *Copaifera langsdorfii* seeds and seed oil. *Bioresource Technology*, *99*(7), 2659–2663.

Sugiyama, J., Vuong, R., & Chanzy, H. (1991). Electron diffraction study on the two crystalline phases occurring in native cellulose from an algal cell wall. *Macromolecules*, *24*(9), 4168–4175.

Tjong, S. C. (2006). Structural and mechanical properties of polymer nanocomposites. *Materials Science & Engineering R: Reports*, *53*(3–4), 73–197.

Tischer, P. C. S. F., Sierakowski, M.-R., Westfahl, H., Jr., & Tischer, C. A. (2010). Nanostructural reorganization of bacterial cellulose by ultrasonic treatment. *Biomacromolecules*, *11*(5), 1217–1224.

Varela-Rizo, H., Weisenberger, M., Bortz, D. R., & Martin-Gullon, I. (2010). Fracture toughness and creep performance of PMMA composites containing micro and nanosized carbon filaments. *Composites Science and Technology*, *70*(7), 1189–1195.

Woehl, M. A., Canestraro, C. D., Mikowski, A., Sierakowski, M.-R., Ramos, L. P., & Wypych, F. (2010). Bionanocomposites of thermoplastic starch reinforced with bacterial cellulose nanofibres: Effect of enzymatic treatment on mechanical properties. *Carbohydrate Polymers*, *80*(3), 866–873.

Wojdyr, M. (2010). Fityk: A general-purpose peak fitting program. *Journal of Applied Crystallography*, *43*(5–1), 1126–1128.

Wong, S.-S., Kasapis, S., & Tan, Y. M. (2009). Bacterial and plant cellulose modification using ultrasound irradiation. *Carbohydrate Polymers*, *77*(2), 280–287.

Woodcock, C., & Sarko, A. (1980). Packing analysis of carbohydrates and polysaccharides. 11. Molecular and crystal structure of native ramie cellulose. *Macromolecules*, *13*(5), 1183–1187.

Yamanaka, S., Yuguchi, Y., Urakawa, H., Kajiwara, K., Shirakawa, M., & Yamatoya, K. (2000). Gelation of tamarind seed polysaccharide xyloglucan in the presence of ethanol. *Food Hydrocolloids*, *14*(2), 125–128.

York, W. S., Harvey, L. K., Guillen, R., Albersheim, P., & Darvill, A. G. (1993). Structural analysis of tamarind seed xyloglucan oligosaccharides using β-galactosidase digestion and spectroscopic methods. *Carbohydrate Research*, *248*, 285–301.

Zhang, Q., Brumers, H., Agren, H., & Tu, Y. (2011). The adsorption of xyloglucan on cellulose: Effects of explicit water and side chain variation. *Carbohydrate Research*, *346*(16), 2595–2602.

Zhou, Q., Rutland, M. W., Teeri, T. T., & Brumer, H. (2007). Xyloglucan in cellulose modification. *Cellulose*, *14*(6), 625–641.